Direct loading of atoms from a macroscopic quadrupole magnetic trap into a microchip trap*

Jun Cheng(程俊)[1,2], Jing-fang Zhang(张敬芳)[1], Xin-ping Xu(许忻平)[1], Hai-chao Zhang(张海潮)[1,†], and Yu-zhu Wang(王育竹)[1,‡]

[1] *Key Laboratory for Quantum Optics, Shanghai Institute of Optics and Fine Mechanics, Chinese Academy of Sciences, Shanghai* 201800, *China*
[2] *University of Chinese Academy of Sciences, Beijing* 100049, *China*

(Received 23 June 2016; revised manuscript received 14 December 2016; published online 23 January 2017)

We demonstrate the direct loading of cold atoms into a microchip 2-mm Z-trap, where the evaporative cooling can be performed efficiently, from a macroscopic quadrupole magnetic trap with a high loading efficiency. The macroscopic quadrupole magnetic trap potential is designed to be moveable by controlling the currents of the two pairs of anti-Helmholtz coils. The cold atoms are initially prepared in a standard six-beam magneto-optical trap and loaded into the macroscopic quadrupole magnetic trap, and then transported to the atom chip surface by moving the macroscopic trap potential. By means of a three-dimensional absorption imaging system, we are able to optimize the position alignment of the atom cloud in the macroscopic trap and the microchip Z-shaped wire. Consequently, with a proper magnetic transfer scheme, we load the cold atoms into the microchip Z-trap directly and efficiently. The loading efficiency is measured to be about 50%. This approach can be used to generate appropriate ultracold atoms sources, for example, for a magnetically guided atom interferometer based on atom chip.

Keywords: atom chip, three-dimensional absorption imaging, direct magnetic loading

PACS: 37.10.Gh, 37.10.Vz, 67.85.–d **DOI:** 10.1088/1674-1056/26/3/033701

1. Introduction

Atom chips[1–4] are very promising tools for the precise control and manipulation of ultracold atoms. By applying modest electric currents on the chip wires, large magnetic field gradients and curvatures can be produced in close proximity to the chips.[5] A variety of trapping,[6] guiding,[7] transporting,[8] and the evaporative cooling[9–11] of cold atoms have been realized on the atom chips. The atoms can be cooled to hundreds of nK after evaporative cooling. And the ultracold atoms are ideally suited for high precision measurement experiments, such as atomic clocks[12] and atom interferometers,[13,14] as well as quantum statistics studies in Bose–Einstein condensate (BEC)[9,10,15] and related degenerate phenomena. In addition, the ultracold atoms held in close proximity to the chip surface are versatile probes for the atom-surface interactions such as the Casimir–Polder interaction,[16] local magnetic fields,[17] and current flow irregularities.[18]

In order to prepare the ultracold atoms, a large number of cold atoms are required to be loaded into a small-volume microchip trap, where the evaporative cooling can be performed efficiently. A typical method is that the atoms are firstly cooled and trapped in a standard six-beam MOT, then magnetically transferred close to the chip surface, and then loaded into the small-volume microchip trap.[15,19] However, various complex transfer wire configurations[10] or intermediate magnetic traps[15,20] are often required during loading the atoms from the macrocopic magnetic trap into the small-volume microchip trap. Therefore, we develop an approach of directly loading cold atoms from a macroscopic quadrupole magnetic trap into a 2 mm-scale microchip Z-trap. Since the evaporative cooling can be performed efficiently in the 2 mm-scale microchip Z-trap even to achieve BEC as shown in the literatures.[9,21,22]

In this paper, we report a direct loading of cold ^{87}Rb atoms into a microchip 2 mm-scale Z-trap from a macroscopic quadrupole magnetic trap (QMT) with a high loading efficiency, and the evaporative cooling in the Z-trap is estimated to be highly efficient. The cold atoms are loaded into the microchip Z-trap by switching the trapping potential from the macroscopic quardrupole potential to the microscopic chip potential gradually, instead of using an additional intermediate magnetic trap. The cold ^{87}Rb atoms are prepared in a standard six-beam MOT firstly, and then loaded into the initial QMT generated by the MOT coils. Then the atoms are moved vertically with the quadrupole magnetic field minimum towards the position near the chip surface, and the detailed process can be seen in our previous work.[23] By switching the trapping potential from the macroscopic quardrupole potential to the microscopic chip potential, the atoms are directly loaded into the microchip 2 mm-scale Z-trap from the final QMT. In addition, we use a three-dimensional absorption imaging system com-

*Project supported by the National Natural Science Foundation of China (Grant No. 11604348).
†Corresponding author. E-mail: zhanghc@siom.ac.cn
‡Corresponding author. E-mail: yzwang@mail.shcnc.ac.cn
© 2017 Chinese Physical Society and IOP Publishing Ltd

bining a grazing incidence imaging setup and an orthogonal-angle-of-incidence imaging setup to precisely optimize the position alignment between the atom cloud and the chip Z-trap. It is beneficial for improving the atom loading efficiency of the microchip Z-trap.

2. Experimental setup and procedure

The experimental setup is illustrated in Fig. 1, and it is based on a single chamber vacuum system. A quartz glass cell of inner size 30 mm × 30 mm × 120 mm is connected with a 40 l/s ion pump, a titanium sublimation pump, and electrical feedthroughs. The vacuum is maintained at a pressure of approximately 1×10^{-8} Pa. The atom chip has dimensions of 14 mm×18 mm, and consists of a 0.25 mm thick silicon dioxide substrate and a 6 μm thick deposited gold layer. To facilitate heat dissipation, the chip is embedded in a copper block. The gold wire pattern of the chip surface is made by the standard photolithographic and electroplating techniques. The leads of the chip wires are connected to the electrical feedthroughs. As shown in Fig. 1(b), the main part of the chip wire pattern includes a Z-shaped wire and a concentric isometric three-ring wire. And the central part of the Z-shaped wire has a length of 2 mm. With an external bias field B_x, the Z-shaped wire can be used to produce a 2 mm-scale Z-trap, which is an Ioffe–Pritchard-type magnetic trap. Figure 2 shows the magnetic potentials created by the Z-shaped wire carrying a current of 3.5 A with three different values of the external x-bias magnetic field: 1.2 mT, 3.5 mT, 6.5 mT, which are the three extreme values used in the experiment. The concentric isometric three-ring wire is used for the toroidal waveguide[24,25] of the ultracold atoms for future experiments.

We use two pairs of partly overlapping anti-Helmholtz coils, which are the MOT and transfer coils, respectively, to transport the atoms from the MOT center to the chip surface.[26–28] The center of the MOT coils is located at 28 mm below the chip surface so that the atom chip does not hinder the six-beam MOT configuration. The QMT can be moved vertically towards the chip surface by increasing the currents in the transfer coils while keeping the currents in the MOT coils constant. We use the three-dimensional printing technology to make the nylon skeleton for the coils, which can eliminate the

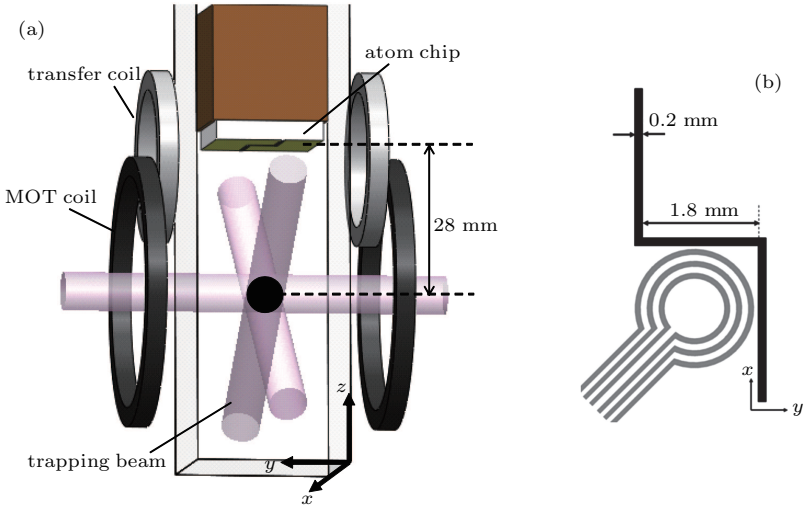


Fig. 1. (color online) Experimental setup. (a) The atoms are captured in a standard six-beam MOT which is 28 mm below the atom chip surface, and then magnetically transported close to the atom chip by the MOT and transfer coils. (b) The main part of wire pattern on the atom chip concludes a Z-shaped wire (black line) and a concentric isometric three-ring wire (grey line). Only the Z-shaped wire is used in the present experiment.

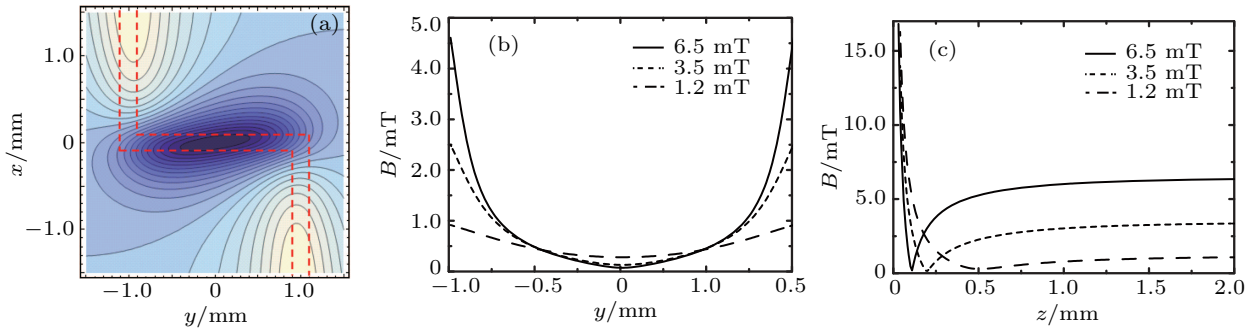


Fig. 2. (color online) (a) The contour map of the magnetic field through the microchip Z-trap center when $I_z = 3.5$ A, $B_{x\text{bias}} = 1.2$ mT in the plane of $z = 0.5$ mm. The red dashed wire presents the chip Z-shaped wire. The magnetic field distribution through the microchip Z-trap center along the y-axis (b) and the z-axis (c), when $I_z = 3.5$ A, and $B_{x\text{bias}} = 1.2$ mT, 3.5 mT, 6.5 mT respectively.

effect of eddy currents that is always an intractable problem for the traditional metal skeleton. In addition, there are also three pairs of Helmholtz coils (not shown in Fig. 1(a)) which are used to generate the homogeneous bias magnetic fields $B_{x\text{bias}}$, $B_{y\text{bias}}$, and $B_{z\text{bias}}$.

The whole experimental procedure mainly consists of three stages, the MOT loading stage, the QMT transport stage, and the microchip trap loading stage. The time sequence is shown in Fig. 3.

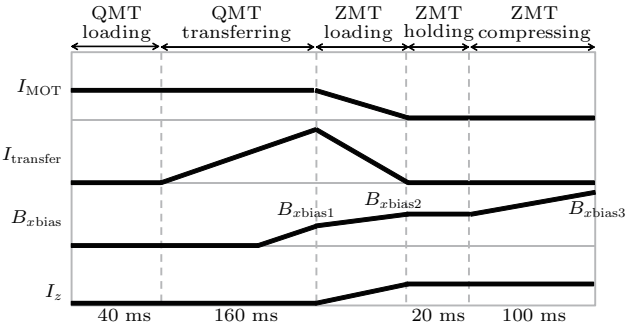


Fig. 3. Time sequence of the atom transport process from the QMT into the chip Z-trap. The ZMT denotes the chip Z-trap.

Initially, the ^{87}Rb atoms are cooled and trapped in the standard six-beam MOT located at 28 mm below the chip surface. The cooling beam is red detuned 12 MHz from the $F = 2 \rightarrow F' = 3$ resonant transition of the ^{87}Rb D_2 line. The beam density of each cooling beam is 18 mW/cm^2 and the beam diameter is 7.5 mm ($1/e^2$). The repumping beam is coupled to the cooling beams and the laser power is 5 mW, with the beam diameter of 7.5 mm $(1/e^2)$. In order to realize efficient loading of atoms into the MOT as well as ultra-high vacuum for a long lifetime in a magnetic trap, we use the light induced atom desorption (LIAD) technique.[29,30] During the MOT loading phase, the UV LEDs are switched on to temporarily increase the rubidium pressure. We collect about 1 $\times 10^8$ cold atoms after a time of 3–4 s. After loading the atoms into the MOT, the UV LEDs are turned off and the atoms are held in the MOT for 3 s to recover the ultrahigh vacuum in the glass cell.

After the MOT loading stage, the atom cloud is compressed within 30 ms. The cooling laser red detuning is increased to 32 MHz and the repumping power is reduced to 1 mW, meanwhile the quadrupole field gradient is increased from 1.4 mT/cm to 4.0 mT/cm. Then we perform a polarization gradient cooling (PGC) process to further cool the atoms within 6 ms. We turn off the currents in the MOT coils, increase the cooling laser red detuning to 72 MHz, and decrease the power of the cooling laser beams to 10 mW simultaneously. The temperature of the atom cloud is about 20 μK after the PGC process. And then the atoms are optically pumped into the $|F = 2, m_F = 2\rangle$ hyperfine ground state. After that, the magnetic field gradient of the MOT coils is increased to 7.3 mT/cm, and the atoms are loaded into the initial QMT produced by the MOT coils. The number and temperature of the atoms in the QMT are $N \sim 7 \times 10^6$ and $T = 110$ μK, respectively.

Then, in the QMT transport stage, the trapped atoms are moved vertically with the magnetic field minimum from the MOT center towards the atom chip surface within 160 ms by increasing the currents in the transfer coils to 26 A linearly and keeping the currents in the MOT coils constant. Simultaneously, the x-bias magnetic field is increased to $B_{x\text{bias1}}$ linearly in the last 50 ms to align the quadrupole trap center with the chip Z-trap center. During the transport process, the atom cloud is compressed gradually, and no obvious loss of atoms is measured. The atom cloud is transferred to about 0.5 mm below the chip surface eventually. The number and temperature of the atoms in the final QMT are $N \sim 7\times10^6$ and $T = 120$ μK, respectively. The Gaussian radius of the atom cloud is 700 μm in the x-axis and z-axis, and 500 μm in the y-axis.

At last, we perform the microchip Z-trap loading after the cold atoms are transferred close to the chip surface. Within a certain loading time t_0, the currents in the MOT and transfer coils are linearly reduced to 0 A, the x-bias magnetic field is ramped from $B_{x\text{bias1}}$ to $B_{x\text{bias2}}$, and the current of the chip Z-shaped wire is increased to 3.5 A linearly. Thus, the trapping potential is switched from the macroscopic quardrupole potential to the microscopic chip potential gradually. As a result, the atoms are loaded into the microchip Z-trap directly.

In order to illustrate the feasibility of the atom loading scheme of the microchip 2 mm-scale Z-trap, we calculate and analyze the magnetic field distribution at different step in the loading process. We set $B_{x\text{bias1}} = 0.3$ mT, $B_{x\text{bias2}} = 1.2$ mT. $B_{x\text{bias}}(t) = (0.3 + 0.9\beta)$ mT, $I_z(t) = 3.5\beta$ A, $I_{\text{MOT}}(t) = 16(1-\beta)$ A, $I_{\text{transfer}}(t) = 26(1-\beta)$ A when the time $t = \beta t_0$ $(0 \le \beta \le 1)$, and t_0 is the loading time interval. As shown in Fig. 4, during the loading process, as the time t increases, the magnetic trap is tighter and tighter, and the trap bottom is raised up gradually. Therefore the atom cloud can be compressed and transferred into the microchip Z-trap from the final QMT gradually. And the loading efficiency can be estimated to be high. The position fluctuation of the magnetic trap center is negligible since it is less than 80 μm and much smaller than the mm-scale of the atom cloud.

The atom cloud in either the macroscopic QMT or the microchip Z-trap is monitored by a three-dimensional absorption imaging system, which combines a grazing incidence imaging setup and an orthogonal-angle-of-incidence imaging setup, as shown in Fig. 5. The two probe beams are both locked to the $F = 2 \rightarrow F' = 3$ resonant transition of the ^{87}Rb D_2 line. In the grazing incidence imaging setup, a probe beam reflects from the chip surface with an angle $\theta = 6^\circ$. The grazing incidence imaging setup gets two images, and their separation d can measure the distance h of the atoms from the chip sur-

face along the z-axis: $h = d/(2\eta\cos\theta)$, and η= 0.7 is the image magnification. The orthogonal-angle-of-incidence imaging setup provides the location of the atom cloud relative to the wire structures on the chip in the x-axis and y-axis. The three-dimensional absorption imaging system can be used to check and optimize the position alignment of the atom cloud trapped in the final QMT with the microchip Z-trap, which can significantly improve the atom loading efficiency of the chip Z-trap.

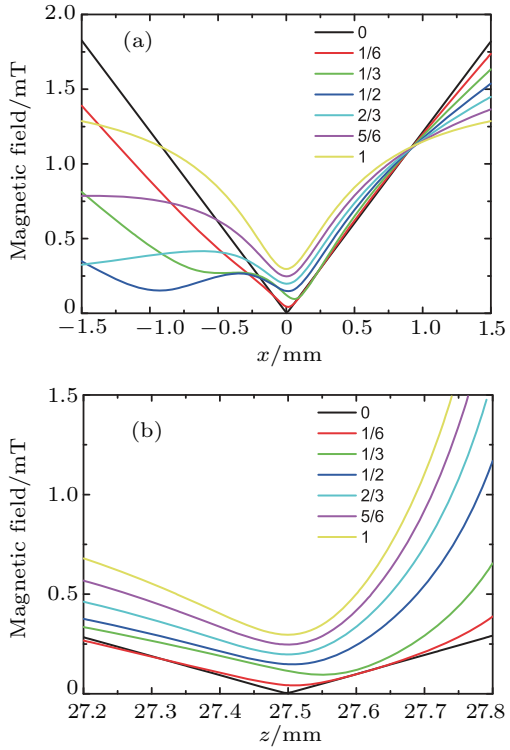


Fig. 4. (color online) (a) Plots of the magnetic field minimum along x-axis (a) and z-axis (b) illustrating the transformation of the final QMT into the microchip Z-trap, where β is 0, 1/6, 1/3, 1/2, 2/3, 5/6, and 1, respectively.

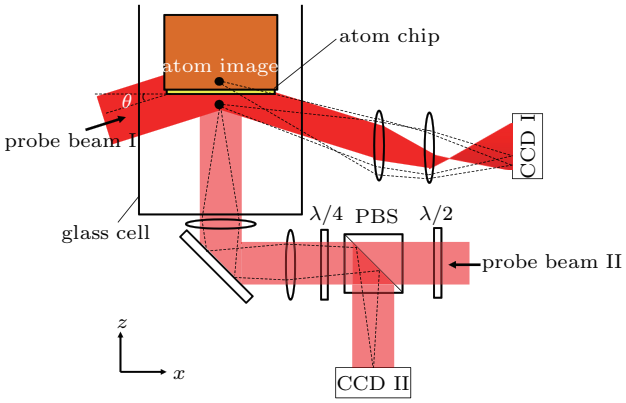


Fig. 5. (color online) Sketch of the three-dimensional absorption imaging system (not to scale).

3. Experimental results and discussion

The atom loading efficiency of the microchip 2 mm-scale Z-trap from the final QMT is influenced by the position deviation between the centers of the atom cloud trapped in the final QMT and the chip Z-trap. The number of atoms loaded into the microchip Z-trap can be approximately estimated to be the atom density times the overlapped volume of the two traps. The scale of the atom cloud is larger than the scale of the microchip trap, especially in the x-direction and z-direction. The scale of the chip Z-trap is 2 mm in the y-direction (also shown in Fig. 2), and the change of the overlapped volume of the two traps can be ignored when the y-bias magnetic field $B_{y\text{bias}}$ is changed. Therefore we mainly adjust the position alignment in the x and z directions precisely in order to maximize the atom number in the chip Z-trap. The optimized way we adopted is changing the $B_{x\text{bias1}}$ in the QMT transferring process and $B_{x\text{bias2}}$ in the chip Z-trap loading process (ZMT process). The former can optimize the position alignment in the x direction and the latter can optimize it in the z direction.

The atom cloud trapped in the final QMT is detected by the orthogonal-angle-of-incidence absorption imaging system. The absorption images of the atom cloud are shown in the Figs. 6(a)–6(c) when $B_{x\text{bias1}}$ is 0 mT, 0.3 mT, and 0.525 mT, respectively. We can see that the chip Z-trap is right above the center of the Z-shaped wire in Fig. 2 (a), so we only need to optimize the position deviation between the centers of the atom cloud trapped in the final QMT and the chip Z-shaped wire in the x-axis and z-axis. From Figs. 6(a) and 6(c), we can see that the atom cloud obviously deviates from the center part of the Z-shaped wire in the x direction. And the atom cloud is aligned to the Z-shaped wire when $B_{x\text{bias1}}$ is 0.3 mT, as shown in Fig. 6(b). When $B_{x\text{bias2}}$ applied in the chip Z-trap loading process is 1.35 mT, the number of atoms loaded into the chip Z-trap changes with $B_{x\text{bias1}}$, as shown in Fig. 6(d). Each data point is the average of five separate measurements and the error bar equals one standard deviation. The optimum atom number can reach 3.5×10^6 when $B_{x\text{bias1}}$ is 0.3 mT, which proves that the atom cloud is aligned to the chip Z-trap center.

The dependence of the atom number in the chip Z-trap on $B_{x\text{bias2}}$ is shown in Fig. 7. Changing the x-bias magnetic field $B_{x\text{bias2}}$ in the chip Z-trap loading stage would change the z-axis location of the trap center, the trap volume and trap depth of the chip Z-trap. The dashed line in Fig. 7 represents the calculated distance between the chip Z-trap center and the chip surface as a function of $B_{x\text{bias2}}$ when $B_{x\text{bias1}} = 0.3$ mT. When $B_{x\text{bias2}}$ is low, the chip Z-trap center deviates from the atom cloud center and the trap depth of the chip Z-trap is rather low, so few atoms are loaded into the chip Z-trap. At a high bias field of $B_{x\text{bias2}}$, the atom number is also decreased because the trap volume of the chip Z-trap is smaller and the position deviation increases. The optimum number of atoms is 3.5×10^6 when $B_{x\text{bias2}}$ is 1.35 mT, which is close to the theoretical calculated value of 1.2 mT when the distance between the chip Z-trap center and the chip surface is 500 μm.

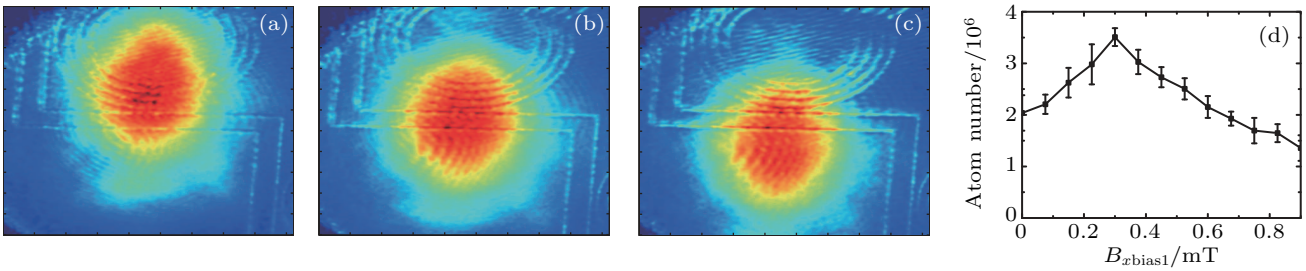


Fig. 6. (color online) The atom cloud in the final QMT is detected by the orthogonal-angle-of-incidence absorption imaging setup: (a) $B_{x\text{bias1}} = 0$, (b) $B_{x\text{bias1}} = 0.3$ mT, (c) $B_{x\text{bias1}} = 0.525$ mT. (d) The number of atoms loaded into the chip Z-trap changes with $B_{x\text{bias1}}$. The solid lines only serve to guide readers.

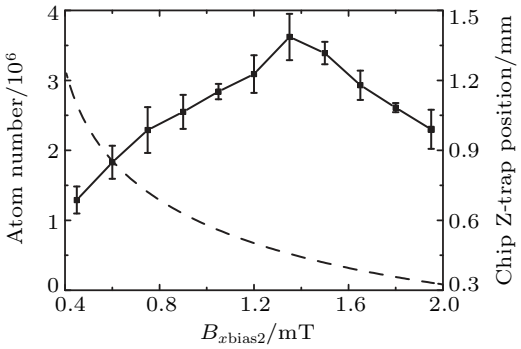


Fig. 7. The atom number in the chip Z-trap changes as a function of $B_{x\text{bias2}}$. The solid lines only serve to guide readers. The dashed curve is the calculated distance between the chip Z-trap center and the chip surface.

The dependence of the number of atoms in the microchip Z-trap as a function of the chip Z-trap loading time is shown in Fig. 8. The data are modeled using the equation[19]

$$\frac{\mathrm{d}N}{\mathrm{d}t} = R\mathrm{e}^{-t/\tau} - \alpha N, \tag{1}$$

where the first term describes loading N atoms into the chip-Z trap at a rate R with a time constant τ during a time t. The second term takes into account the loss of atoms during the trap loading. An additional loss term due to collisions between cold trapped atoms is not considered because of the relatively low density ($\sim 10^{10}$ m^{-3}) of the atom cloud. We can derive the general solution of Eq. (1) as

$$N = \frac{R\tau}{\alpha\tau - 1}(\mathrm{e}^{-t/\tau} - \mathrm{e}^{-\alpha t}). \tag{2}$$

The best fit of Eq. (2) to the data gives $R = 3.8 \times 10^8$, $\tau = 0.3$ s, $\alpha = 0.19$ s, and the best loading time we derived is 5.2 ms.

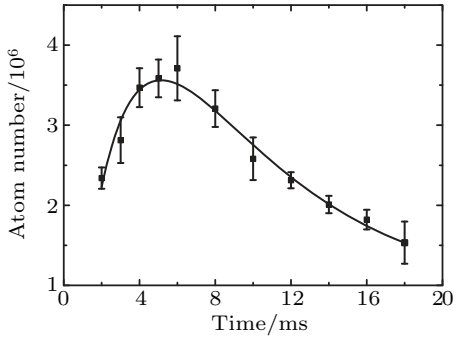


Fig. 8. Dependence of number of atoms in the chip Z-trap on the loading time. The solid curve is fit to the data using Eq. (2).

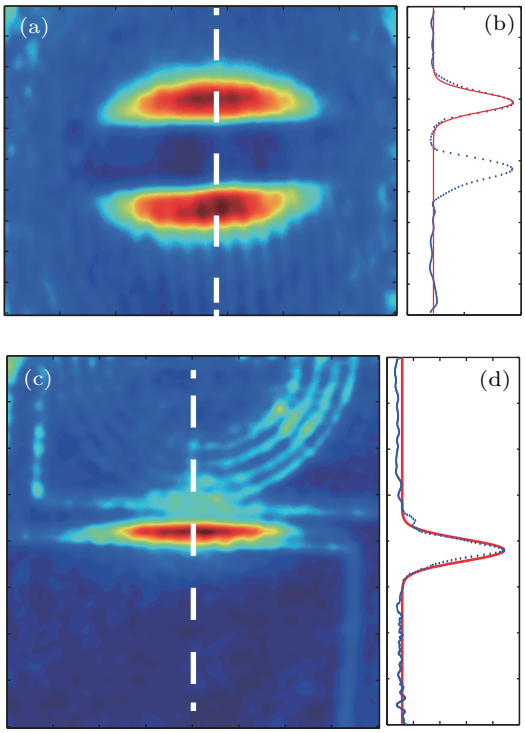


Fig. 9. (color online) Absorption images of the atoms trapped in the microchip Z-trap when $I_z = 3.5$ A, $B_{x\text{bias3}} = 6.5$ mT. The atom images are detected by the Grazing incidence imaging (a) and the orthogonal-angle-of-incidence imaging system (c). The profile of the atom cloud along the vertical dashed line is also shown in panels (b) and (d), respectively. The solid red curve is a Gaussian profile fitted to the data.

Finally, the atom transport efficiency achieves 50% from the macroscopic QMT to the microchip 2 mm-scale Z-trap after optimizing the experimental parameters. The number and temperature of the loaded atoms are $N \sim 3.5 \times 10^6$ and $T \sim 300$ μK, respectively. After the initial loading of the chip-Z trap, we can compress the trap and make the atoms closer to the chip surface by keeping the chip Z-wire current 3.5 A and increasing the x-bias magnetic field to $B_{x\text{bias3}}$ (6.5 mT). The atom cloud is about 100 μm away from the chip surface. The absorption images of the atomic cloud in the compressed microchip Z-trap are shown in Fig. 9. The atom density distribution in the vertical x direction is fitted by a Gaussian function, and the Gaussian radius of the atom cloud is 75 μm along the x-axis, 730 μm along the y-axis. The phase density of the cloud is 4.4×10^{-6}. The magnetic trap frequency is (5370, 26,

5370) Hz, and the elastic collision rate is estimated to be high enough for efficient evaporative cooling. In the future experiment, the ultracold atoms can be further transferred into the toroidal magnetic guide by adjusting the three directional bias magnetic fields after the evaporative cooling.

4. Conclusion

We have demonstrated a simple and efficient loading of cold atoms from a standard six-beam MOT into a 2 mm-scale microchip Z-trap. The atoms are firstly loaded into the standard six-beam MOT, then transferred vertically 27.5 mm up to the position near the chip surface after a simple QMT transport stage. Finally, the cold atoms are loaded into the microchip Z-trap by switching the trapping potential from the macroscopic quardrupole potential to the microscopic chip potential gradually, instead of using an additional intermediate magnetic trap. We have calculated and analyzed the magnetic field distribution at different steps in the microchip Z-trap loading process, and proved the feasibility of the direct atom loading scheme. We studied the mode-match between the macro QMT and the microchip 2 mm-scale Z-trap, and maximized the chip Z-trap loading efficiency by optimizing the transfer scheme and precisely adjusting the position alignment of the traps with the help of the three-dimensional absorption imaging system. Finally, we loaded 3.5×10^6 atoms into the 2 mm-scale microchip Z-trap, and the loading efficiency achieved 50%. We also further compressed the chip Z-trap and the atom cloud was about 100 μm away from the chip surface, the corresponding elastic collision rate is estimated to be high enough for the efficient evaporative cooling. This approach could be used to generate appropriate ultracold atoms sources, for example, for a magnetically guided atom interferometer based on atom chip. The work also paves the way for studying the interaction of ultracold atoms with surfaces and quantum devices based on atom chips.

References

[1] Reichel J, Hänsel W and Hänsch T W 1999 *Phys. Rev. Lett.* **83** 3398

[2] Feenstra L, Andersson L M and Schmiedmayer J 2004 *Gen. Relat. Gravit.* **36** 2317

[3] Folman R, Kruger P, Cassettari D, Hessmo B, Maier T and Schmiedmayer J 2000 *Phys. Rev. Lett.* **84** 4749

[4] Reichel J, Hänsel W, Hommelhoff P and Hänsch T W 2001 *Appl. Phys. B: Lasers Opt.* **72** 81

[5] Weinstein J D and Libbrecht K G 1995 *Phys. Rev. A* **52** 4004

[6] Reichel J 2002 *Appl. Phys. B: Lasers Opt.* **74** 469

[7] Dekker N H, Lee C S, Lorent V V, Thywissen J H, Smith S P, Drndic M, Westervelt R M and Prentiss M 2000 *Phys. Rev. Lett.* **84** 1124

[8] Hänsel W, Reichel J, Hommelhoff P and Hänsch T W 2001 *Phys. Rev. Lett.* **86** 608

[9] Hänsel W, Hommelhoff P, Hänsch T W and Reichel J 2001 *Nature* **413** 498

[10] Ott H, Fortagh J, Schlotterbeck G, Grossmann A and Zimmermann C 2001 *Phys. Rev. Lett.* **87** 230401

[11] Du S W and Oh E 2009 *Phys. Rev. A* **79** 013407

[12] Maineult W, Deutsch C, Gibble K, Reichel J and Rosenbusch P 2012 *Phys. Rev. Lett.* **109** 020407

[13] Wang Y J, *et al.* 2005 *Phys. Rev. Lett.* **94** 090405

[14] Abend S, *et al.* 2016 *Phys. Rev. Lett.* **117** 203003

[15] Horikoshi M and Nakagawa K 2006 *Appl. Phys. B* **82** 363

[16] Lin Y J, Teper I, Chin C and Vuletic V 2004 *Phys. Rev. Lett.* **92** 050404

[17] Jones M P A, Vale C J, Sahagun D, Hall B V, Eberlein C C, Sauer B E, Furusawa K, Richardson D and Hinds E A 2004 *J. Phys. B: At. Mol. Opt. Phys.* **37** 15

[18] Aigner S, Della Pietra L, Japha Y, Entin-Wohlman O, David T, Salem R, Folman R and Schmiedmayer J 2008 *Science* **319** 1226

[19] Jian B and van Wijngaarden W A 2013 *J. Opt. Soc. Am. B* **30** 238

[20] Farkas D M, Hudek K M, Salim E A, Segal S R, Squires M B and Anderson D Z 2010 *Appl. Phys. Lett.* **96** 093102

[21] Du S, Squires M B, Imai Y, Czaia L, Saravanan R A, Bright V, Reichel J, Hänsch T W and Anderson D Z 2004 *Phys. Rev. A* **70** 053606

[22] Yan B, Cheng F, Ke M, Li X L, Tang J Y and Wang Y Z 2009 *Chin. Phys. B* **18** 4259

[23] Cheng J, Xu X, Zhang J, Chen Y, Zhang H and Wang Y 2016 *Acta Opt. Sin.* **36** 1202001 (in Chinese)

[24] Jiang X J, Li X L, Xu X P, Zhang H C and Wang Y Z 2015 *Chin. Phys. Lett.* **32** 020301

[25] Wu S, Su E and Prentiss M 2007 *Phys. Rev. Lett.* **99** 173201

[26] Han J S, Xu X P, Zhang H C and Wang Y Z 2013 *Chin. Phys. B* **22** 023702

[27] Gao K Y, Luo X Y, Jia F D, Yu C H, Zhang F, Yin J P, Xu L, You L and Wang R Q 2014 *Chin. Phys. Lett.* **31** 063701

[28] Zhang F, Long Y, Yang J L, Ma G Q, Yin J P and Wang R Q 2015 *Chin. Phys. Lett.* **32** 123701

[29] Klempt C, van Zoest T, Henninger T, Topic O, Rasel E, Ertmer W and Arlt J 2006 *Phys. Rev. A* **73** 013410

[30] Torralbo-Campo L, Bruce G D, Smirne G and Cassettari D 2015 *Sci. Rep.* **5** 14729